

Role of Tumor Microvessel Architecture and Function in Chemotherapeutic Drug Delivery: A Three-Dimensional Numerical Study

Yan Cai¹¹, Zhiyong Li^{1,2*}

Abstract: To investigate the dynamic changes of solid tumor and neo-vasculature in response to chemotherapeutic agent, we proposed a multi-discipline three-dimensional mathematical model by coupling tumor growth, angiogenesis, vessel remodelling, microcirculation and drug delivery. The tumor growth is described by the cell automaton model, in which three cell phenotypes (proliferating cell, quiescent cell and necrotic cell) are assumed to reflect the dynamics of tumor progress. A 3D tree-like architecture network with different orders for vessel diameter is generated as pre-existing vasculature in host tissue. The chemical substances including oxygen, vascular endothelial growth factor, extra-cellular matrix and matrix degradation enzymes are calculated based on the reaction-diffusion equations associated with haemodynamic environment, which is obtained by coupled modelling of intravascular blood flow with interstitial fluid flow. The haemodynamic changes, including vessel diameter and permeability, are introduced to reflect a series of pathological characteristics of abnormal tumor vessels involving vessel dilation, leakage, angiogenesis, regression and collapse. The chemotherapeutic drug is transported across the vessel wall and through diffusion and convection mechanisms in the interstitial media, which is governed by the second Fick's law. Finally, we coupled the tumor growth model and the vessel remodelling model according to the changes in the chemical and hemodynamical microenvironment, to investigate the tumor inhibition with different drug strategies. The results showed the growth histories of tumor cell population in response to chemotherapeutic agent. The efficacies of tumor inhibition by different drug strategies had been compared. In addition, we studied the influences of the pathological abnormalities of tumor microvessels, such as high density, heterogeneous capillary diameter and high permeability of vessel wall, on the drug transport and chemotherapeutic efficacy.

Keywords: Mathematical modelling of drug delivery, three-dimensional capillary network, tumor growth, microvessel structure and function.

¹ School of Biological Science and Medical Engineering, Southeast University, Nanjing, 210096, China.

² School of Chemistry, Physics and Mechanical Engineering, Science and Engineering Faculty, Queensland University of Technology, 2 George St, Brisbane City, QLD 4000, Australia.

*Corresponding author: Zhiyong Li, Southeast University, Nanjing China, email: zylicam@gmail.com.

1 Introduction

Cancer, as a leading cause of compromised quality of life and death, results from uncontrolled proliferation of mutated cells. During the early stage of the growing cell mass, nutrients supply to the hyperplasia tissue predominantly comes from the pre-existing vasculature supplying the surrounding healthy tissues. This stage of development of a primary tumor is known as avascular phase. As the tumor exceeds a critical size ($1-2\text{mm}^3$) [Viallard and Larrivé (2017)], it must induce the development of its own vasculature to supply its growth—a process known as angiogenesis. This process may involve the extension of pre-existing blood vessels, and/or recruitment of circulating endothelial progenitor cells. Regardless of its origins, all tumor vasculature has abnormal pathophysiological characteristics in both architecture and function [Fukumura and Jain (2007)]. Different from the well-organized architecture of normal microvessels, tumor vessels are dilated, tortuous, chaotic, and heterogeneous in their spatial distribution. Vessel wall structure is also abnormal in tumors, including lack of normal basement membrane and large inter-endothelial junctions [Danhier, Feron and Preat (2010)]. Abnormalities in vascular architecture result in the pathological blood perfusion and vascular function [Eberhard, Kahlert and Goede et al. (2000)]. For example, the tortuous geometry of tumor microvessels increases the resistance to blood flow, leading to low overall perfusion rate, and spatial and temporal heterogeneity in tumor blood perfusion. The leaky vessel wall and the lack of lymphatic drainage both contribute to the elevated tumor interstitial fluid pressure (IFP) [Rofstad, Galappathi and Mathiesen (2014)].

The abnormal tumor vasculature causes abnormal microenvironment and hinders the drug delivery to tumors [Narang and Varia (2011)]. Once the systemically administered drugs have reached the tumor vasculature, they must transport within the blood flow, cross the vessel wall and diffuse through the interstitial space to reach the tumor cells. The average tumor blood flow is lower than normal tissues [Jain (1990)], which influences the drug delivery inside the tumor vessels. Transvascular drug transport in tumors is associated with the transvascular fluid flow across the vessel wall, which is governed by the hydrostatic and osmotic pressure differences between the blood vessel and the interstitial space [Knawar, Kim and Kuh (2015)]. In fact, the high IFP in the tumor due to the abnormal leaky vessel can decrease the convection across tumor vessel walls. As a result, IFP is uniformly high throughout a tumor and drops dramatically in the tumor margin. Therefore, the uniformly elevated IFP compromises the drug delivery both across the vessel wall and interstitium in tumors [Boucher, Baxter and Jain (1990)]. In conclusion, although the abnormal vasculature could support tumor delivery of macromolecules by contributing to the enhanced permeation and retention (EPR) effect [Maeda et al. (2000)], they hinder the delivery and efficacy of therapeutic agents to tumors.

Due to practical limitations, much of our understanding of the effects of chemotherapeutic drugs on tumors is based on *in vitro* experiments using monolayer cultures or multicellular spheroids [Xu, Farach-Carson and Jia (2014); Seo, DelNero and Fischbach (2014)]. Nowadays, mathematical models based on underlying biological properties can provide a powerful tool to facilitate the quantitative understanding of the dynamics of how drugs get to and penetrate through the tumor mass. Early studies of *in silico* modeling of drug delivery to solid tumors basically considered the distribution of variables, such as interstitial pressure and concentration, over the length scale of the spherical tumor [Mishra, Katiyar and Arora (2007)];

Sefidgar et al. (2014)]. They often used a continuum media model to simulate the solute transport and the interstitial flow. Developed models focused on the effect of heterogeneous tissue transport properties on interstitial transport [Sefidgar et al. (2015); Moghadam et al. (2015)]. The introduction of discrete microvascular network models helped us to incorporate drug transport with spatial and temporal variations in blood flow. In addition, coupled hemodynamic models of intravascular flow with the interstitial flow improved the solutions of IFP and fluid flow in the intravascular, transvessel and interstitial domains, to provide better tools on studying drug delivery [Tang et al. (2014)]. The rapid developments of mathematical modeling of drug transport in tumors have also focused on investigating the effects of dynamic microenvironment on the solute distribution. The influence of vessel wall permeability and vascular heterogeneities on drug delivery was reported by Welter and Rieger [Welter and Rieger (2013)]. Sefidgar et al. [Sefidgar et al. (2015)] presented a mathematical model to study drug delivery in a dynamic tumor microvasculature by considering a remodeling network based on hemodynamic and metabolic stimuli. Penta et al. [Penta and Ambrosi (2015)] studied the role of vessel tortuosity in macroscale tumor blood flow by solving the homogenized fluid transport model. However, the tumor growth was not included in above works and the coupling response between tumor growing with the changed microenvironment due to therapeutic drugs was not considered. Tang et al. [Tang et al. (2014)] proposed a comprehensive computational model by coupling tumor growth and angiogenesis to simulate tumor progression for chemotherapy evaluation. They focused on the solid tumor geometry and ignored the dynamic behavior of capillaries.

In the previous work of our group, a fully coupled mathematical model of tumor growth, angiogenesis and blood perfusion was established [Cai et al. (2011)] and further developed to apply on a brain tumor by incorporating glioblastoma growth, pre-existing vessel co-option, angiogenesis and blood flow [Cai, Wu and Li et al. (2016)]. In the present work, the drug delivery modeling system is introduced in our coupled model to investigate the dynamic changes of solid tumor and neo-vasculature in response to chemotherapeutic agent. We apply cytotoxic drugs such as Cisplatin that directly act at the tumor cell and induce damage to cell DNA to prevent cell replication. The dynamics of drugs as well as other chemicals (Oxygen, VEGF, ECM and MDE) are modeled using partial differential equations. The chemical microenvironment is coupled with hemodynamical microenvironment, which includes intravascular blood perfusion and interstitial fluid field. We describe the tumor growth by using the probabilistic cell automaton model in which the different cell behaviors are assumed to be associated with local microenvironment. In addition, the pathological abnormalities of tumor microvessels, such as high density, heterogeneous capillary diameter and high permeability of vessel wall, are analyzed in the current mathematical model. The influence of these factors on the drug transport and chemotherapeutic efficacy is also studied quantitatively.

2 Material and methods

2.1 Generation of tumor microvasculature and chemical microenvironment

In the present model, a uniformly distributed grid of $100 \times 100 \times 100$ is generated in a

cube simulation domain of 1 mm^3 , i.e., the length between the neighboring nodes is $10 \text{ }\mu\text{m}$. The pre-existing vasculature has a typical parallel architecture network along y axis according to the features of microvascular in normal tissue (Fig. 1A).

A three-dimensional hybrid discrete-continuum angiogenesis model is introduced to investigate the endothelial cell migration and proliferation through random motility, chemotaxis in response to VEGF distributions and haptotaxis in response to the local ECM density. All endothelial cells have a probability P_{spr} to sprout and trigger angiogenesis when the local VEGF concentration exceeds a threshold θ_{spr} . The endothelial cell distribution (denoted by e) is updated based on the equation

$$\frac{\partial e}{\partial t} = \underbrace{D_e \nabla^2 e}_{\text{diffusion}} - \nabla \cdot \left(\underbrace{\frac{\phi_c}{1 + \sigma C_v} e \nabla C_v}_{\text{chemotaxis}} + \underbrace{\phi_h e \nabla C_f}_{\text{haptotaxis}} \right) \quad (1)$$

where D_e , ϕ_c and ϕ_h are EC diffusion, chemotaxis and haptotaxis coefficients, respectively. C_v and C_f are concentrations of VEGF and ECM respectively, and satisfy the following equations

$$\frac{\partial C_v}{\partial t} = D_v \nabla^2 C_v + \chi TC_{i,j} + \xi C_f - \varepsilon EC_{i,j} - \lambda_v C_v \quad (2)$$

$$\frac{\partial C_f}{\partial t} = -\delta C_m C_f \quad (3)$$

The $TC_{i,j}$ and $EC_{i,j}$ terms represent a tumor cell (TC) and an endothelial cell (EC) located at a node position (i, j) . Their values are either 1 if a cell is present or 0 if it is not. D_v is VEGF diffusion coefficient. χ , ξ , ε , λ_v , δ are positive constants. C_m is the concentration of matrix degradation enzymes (MDEs), and satisfies

$$\frac{\partial C_m}{\partial t} = D_m \nabla^2 C_m + \mu_T TC_{i,j} + \mu_E EC_{i,j} - \lambda_m C_m \quad (4)$$

where D_m is the MDE diffusion coefficient. μ_T , μ_E , λ_m are positive constants.

We used the Euler's nine points finite difference scheme to discretize the Eq. (1) [Cai, Xu and Wu et al. (2011); Anderson and Chaplain (1998)], in which the discretized equation of ECs was:

$$\begin{aligned} n_{i,j,k}^{q+1} = & n_{i,j,k}^q P_0 + n_{i+1,j,k}^q P_1 + n_{i-1,j,k}^q P_2 + n_{i,j+1,k}^q P_3 + n_{i,j-1,k}^q P_4 \\ & + n_{i,j,k+1}^q P_5 + n_{i,j,k-1}^q P_6 \end{aligned} \quad (5)$$

where the subscripts i, j, k and the superscripts q specify the location on the grid and the time steps, respectively. We assume that the coefficients $P_0 \sim P_6$ are the probability density functions to determine the movement directions of the sprouts. The seven coefficients correspond to the seven possible movements for ECs, including stationary and move along the six directions in a three dimensional space (Fig.1B). In each time step, the

probability density function $P_0 \sim P_6$ can be integrated into the cumulative distribution function. The probability of the EC to migrate to the certain neighbor grid is set to be proportional to the value of the cumulative distribution function. After the ECs distribution updated, there are two 3D binary matrixes A and B to record the topology of the vessel network. The former is imposed on the simulation grids, while the latter on the vessel segments. The values of both are 1 if the EC/vessel is on the grid/segment, and 0 if it is not.

The new sprouts are assumed to generate only from the existing sprout tips, and the newly formed sprouts are unlikely to branch immediately. Sufficient space locally is requisite for the forming of a new sprout. Furthermore, we assume that the probability of generating a new sprout is dependent on the local concentration of VEGF, i.e., $P_{spr} \propto C_V$. If one sprout tip encounters another sprout or vessels, anastomosis will occur. As a result of the tip-to-tip fusions, only one of the original sprouts continues to grow.

We classify the vessel branches according to the Strahler system, a well-established method for describing stream order (Fig.1C). In Strahler's system, leaf segments are assigned Strahler order one. The Strahler order will increase when two vessels with the same Strahler orders join into one vessel. However, two vessels with different Strahler order meeting will not create a vessel with higher order. In our model, there are three Strahler orders to show the branching pattern. Different vessel diameters and collapse pressure of vessel segments P_c (see Section 2.2 for details) are defined corresponding to three Strahler orders to reflect the heterogeneous characteristic of the tumor microvasculature (Table 1).

Table 1: The diameter and average length, and the collapse pressure of vessel segments of different Strahler orders.

Strahler order	1	2	3
Diameter (μm) [Cassot, Lauwers and Fouard et al. (2006)]	8	12	16
Length (μm) [Cassot, Lauwers and Fouard et al. (2006)]	80	200	320
P_c (mmHg) [Deisboeck, Berens and Kansal et al. (2001)]	1.0	1.5	2.0

The oxygen transport inside the vessel is represented by the advection equation subject to the equilibrium of the free and bound oxygen:

$$\frac{\partial C_{o_F}^{in}}{\partial t} = -\vec{U}_v \cdot \nabla C_{o_F}^{in} \tag{6}$$

$$\frac{\partial C_{o_B}}{\partial t} = -\vec{U}_v \cdot \nabla C_{o_B} \tag{7}$$

$$C_{o_B} = 4H \cdot C_{Hb} \cdot SO_2(C_{o_F}^{in}) \tag{8}$$

where $C_{o_F}^{in}$ and C_{o_B} are the free and bound oxygen concentrations inside the vessel, respectively. \vec{U}_v denotes the intravascular blood velocity; H denotes haematocrit obtained from the haemodynamic calculation; C_{Hb} is the haemoglobin concentration

within a red blood cell; $SO_2(C_{o_F})$ is the haemoglobin oxygen saturation [Fang et al. (2008)].

The free oxygen flux across the vessel wall satisfies the Fick's law:

$$\frac{\partial C_{o_F}^{ex}}{\partial t} V = J \cdot A \quad (9)$$

where $C_{o_F}^{ex}$ is the free oxygen concentration in the tissue space. V and A are the tissue volume and the associated vessel wall area. J is the oxygen flux which is obtained by

$$J = -L_p \frac{(C_{o_F}^{ex} - C_{o_F}^{in})}{\alpha w} \quad (10)$$

where α is the Bunsen solubility coefficient; w is the vessel wall thickness. L_p is the vessel wall permeability which is varied in different maturity level of vessel segments.

The interstitial fluid velocity is very slow due to the low interstitial pressure gradient in the tumor region. In fact, U_i is almost 100 times smaller than U_v in value according to the simulation results in our previous model. Therefore, we assume the free oxygen transported through the tissue space is governed only by the oxygen diffusion equation which is not influenced by the interstitial fluid velocity U_i .

$$\frac{\partial C_{o_F}^{ex}}{\partial t} = \nabla \cdot (D_o \nabla C_{o_F}^{ex}) - \gamma TC_{i,j} \quad (11)$$

where D_o is the tissue oxygen diffusion coefficient and γ is the consumption co-efficient.

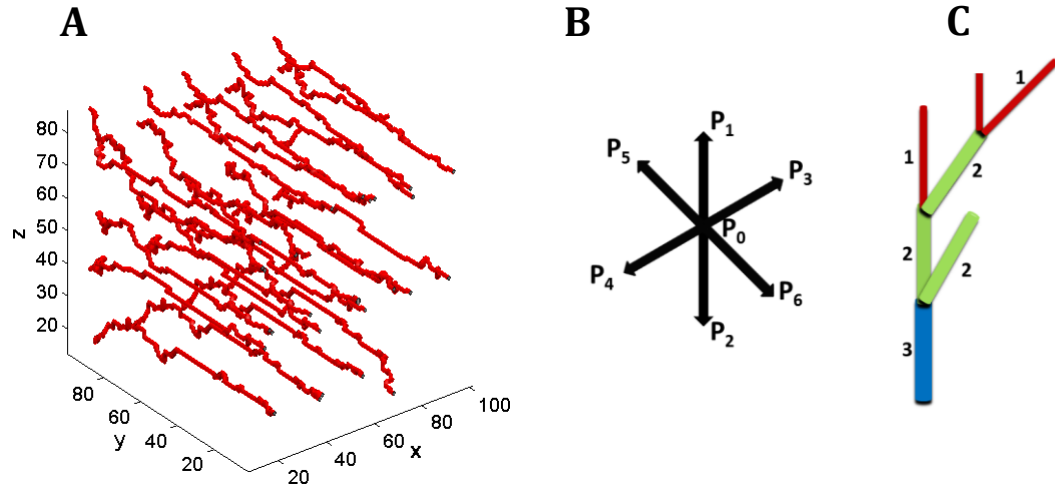


Figure 1: (A) A three-dimensional pre-existing vasculature with a typical parallel architecture network along y axis according to the features of microvascular in normal tissue. A uniformly distributed grid of $100 \times 100 \times 100$ is generated in a cube simulation domain of 1 mm^3 , i.e., the length between the neighboring nodes is $10 \mu\text{m}$. (B) P_0 – P_6 are the probability density functions to determine the seven possible movement directions of the sprouts, including stationary and move along the six directions in a three dimensional space. C: The schematic of a typical Strahler system, which is used to classify the

branches of the microvasculature.

2.2 Coupled hemodynamic calculation

The calculation of hemodynamics in microcirculation incorporates three parts, which are (a) intravascular blood flow; (b) interstitial fluid flow and (c) transvascular flow. Briefly, for the intravascular blood flow, the governing equation is the flux conservation at each node. The incompressible blood flow satisfies the Poiseuille's law. The interstitial area is assumed to be a porous media, while the interstitial fluid follows the Darcy's law. We coupled the intravascular and interstitial flow by updating the transvascular flow, which is controlled by the Starling's law. Blood viscosity is a function of vessel diameter, local haematocrit, and plasma viscosity ^[24]. In addition, vessel compliance and wall shear stress are correlated to vessel remodeling and vessel collapse. The detailed illustrations for coupled modeling of hemodynamic calculation can be found in Wu et al. [Wu, Long and Xu et al. (2009)].

The main equations for blood flow calculation are as follows:

$$Q_v = \frac{\pi R^4 \Delta P_v}{8 \mu \Delta l} \quad (12)$$

$$Q_t = 2\pi R \cdot \Delta l \cdot L_p (P_v - P_i - \sigma_T (\pi_v - \pi_i)) \quad (13)$$

$$Q = Q_v - Q_t \quad (14)$$

where Q is the flow rate of each vessel segment, which has a value zero at each node of the vessel network due to the assumption of flux conservation and incompressible flow. Q_v is the vascular flow rate without fluid leakage; Q_t is the transvascular flow rate. Δl and R are the mean length and radius of the vessel segment. P_v and P_i are the intravascular pressure and the interstitial pressure, respectively. L_p is the hydraulic permeability of the vessel wall. σ_T is the average osmotic reflection coefficient for plasma proteins; π_v and π_i are the colloid osmotic pressure of plasma and interstitial fluid, respectively.

The velocity of intravascular U_v and interstitial flow U_i satisfies

$$U_v = Q / \pi R^2 \quad (15)$$

$$U_i = -K \nabla P_i \quad (16)$$

$$\nabla \cdot U_i = \frac{L_p S}{V} (P_v - P_i - \sigma_T (\pi_v - \pi_i)) \quad (17)$$

where K is the hydraulic conductivity coefficient of the interstitium; S/V is the surface area per unit volume for transport in the interstitium.

In our model, the dynamics of vessel remodeling includes vessel dilation, vessel compression and collapse [Cai, Wu and Li et al. (2016)]. In brief, a high local VEGF concentration will cause a vessel segment inside the tumor to be dilated which will cause an increase in vessel wall permeability and a decrease in vessel collapsing pressure. In this way, vessel may be compressed due to the increased interstitial pressure. A vessel with a changed diameter will influence local wall shear stress (WSS). We assume that a

vessel segment will collapse if the local WSS is too low for a long period. The detailed model assumptions and parameter setting will be addressed in the following paragraphs.

A vessel segment inside the tumor that has a VEGF concentration larger than a threshold θ_{VEGF} will increase its radius R with the rate of $0.4\mu\text{m/h}$ which will stop when the vessel radius reaches the maximum value of $R_{\text{max}}=10\mu\text{m}$. At the same time, the permeability of the vessel wall L_p is increasing in a dilation vessel, and satisfies

$$L_p = \begin{cases} L_p^T \left(\frac{R}{R_{\text{max}}} \right), & \text{immature vessel} \\ L_p^N, & \text{mature vessel} \end{cases} \quad (18)$$

where L_p^N is the initial value of L_p referred to the vessel permeability value in the normal tissue; L_p^T is the maximum value of L_p according to the experiments of vessel permeability value in a tumor microvessel.

The pressure value that will cause a vessel to collapse is defined as P_c which represents the ability of a vessel segment remaining structurally intact under the trans-wall pressure difference. In this study, initial P_c values were predefined for each vessel according to the Strahler order of the vessel segment in the pre-existing vessel network. The vessel with the larger diameter has a higher initial P_c (Table 1). When the local microenvironment was changed by the proliferating tumor cells, Ang-2 is up-regulated in co-opted vessels, causing the destabilization of the vessel wall, i.e., the detachment of pericytes from the endothelial tube [Holash, Maisonpierre and Compton et al. (1999)]. Since the Ang-2 concentration and pericyte density are not included in this model, we assume that P_c decreases with increasing permeability of vessel wall L_p in the immature vessel.

$$P_c = P_c^{\min} \left(\frac{L_p^T}{L_p} \right) \quad (19)$$

where P_c^{\min} is the smallest collapse pressure that an immature vessel segment can have, and set to be $0.5P_c$ of different Strahler orders.

For a pre-existing vessel, once vessel dilation occurs, the vessel segment is treated as an immature vessel with increased L_p and decreased P_c . In the simulation, vessel wall compliance is defined by the radius changing under the influence of intravascular and interstitial pressures and collapse pressure based on the empirical equation of Netti et al [Netti, Roberge and Boucher et al. (1996)].

$$R = \begin{cases} R_0 \left(\frac{P_v - P_i + P_c}{E} \right)^b, & \text{immature vessel} \\ R_0, & \text{mature vessel} \end{cases} \quad (20)$$

where R_0 is the origin radius of the capillary; b is the compliance exponent; E is the compliance coefficient.

The three variables R , L_p and P_c are fully coupled in the model [Cai, Wu and Li et al. (2016)]. In the simulation of vessel remodelling, we first solved Eq. (18) for all immature vessels, i.e., dilated vessels, to obtain the values of L_p . Then we perform the haemodynamic calculation with updated L_p to obtain P_i , and also solved Eq. (19) to obtain P_c . Finally, we updated vessel radius R for the iteration by P_i and P_c according to Eq. (20).

Based on the above equations, when the vessel segment becomes immature, L_p will increase which causes lower P_c , and consequently P_i will increase, both of the changes can cause vessel compressing. A compressed vessel, on the other hand will induce a higher flow resistance, lower flow which will then decrease the wall shear stress (WSS) level for the vessel. Vessel collapse will occur by either WSS criteria (as described below) or a significant reduced R.

As defined in our previous work and others' that vessel will collapse due to a long period of low WSS status in which the apoptosis of EC dominate the collapse process [Cai, Xu and Wu et al. (2011); Welter, Bartha and Rieger (2009)]. WSS is used to estimate this kind of vessel regression. The WSS of a vascular segment can be calculated as

$$\tau = \frac{\Delta P_v \cdot R}{2\Delta l} \quad (21)$$

We assume that a circulated vessel, which is surrounded by the TCs, will collapse with a pre-defined probability if the WSS value in the vessel is $<1/2f_0$ where f_0 is the mean WSS value in the vessels of Strahler order 3 in the entire model. The probability is assumed to be proportional to the duration of low WSS in the vessel, i.e., the longer the vessel experiences the low WSS, the more likely the vessel is to collapse if the criterion is satisfied.

2.3 Drug delivery

The drug transport is due to diffusion and convection mechanisms in interstitial media. The former is calculated according to first Fick's law and the latter is influenced by the interstitial fluid velocity which is obtained by the hemodynamics calculation. In addition, the sources and sinks for drugs in tumor tissues should be considered in the model. Therefore, by applying the second Fick's law, the mass conservation equation for drug transport can be written as

$$\frac{\partial C_d}{\partial t} = \nabla \cdot (D_d \nabla C_d) - \nabla (U_i C_d) + \phi_V - \phi_L \quad (22)$$

where C_d is the drug concentration; D_d is drug diffusion coefficient; ϕ_V is the source item, i.e., the rate of drug transport per unit volume from blood vessel into the interstitial space, and ϕ_L is the sink item, i.e., the rate of drug transport per unit volume from the interstitial space into the lymph vessels.

The transvascular movement of drugs from vessel wall to interstitium occurs in the form of both diffusion and convection. The diffusion transport is caused by concentration gradient of drugs between plasma and interstitium. The convective transport of drugs is associated with the pressure gradient across the vessel wall. We use the equation proposed by Patlak et al. [Patlak, Goldstein and Hoffman (1963)] to describe the transvascular delivery from vessel to tissue:

$$\phi_V = \underbrace{L_p \frac{S}{V} (C_d^P - C_d) \left[\frac{P_{ec}}{e^{P_{ec}} - 1} \right]}_{diffusion} + \underbrace{\phi_V (1 - \sigma_f) C_d^P}_{convection} \quad (23)$$

where C_d^P is the drug concentration in plasma and σ_f is the solvent-drag reflection coefficient. P_{ec} is the Peclet number, indicating the ratio of convection to diffusion

effect across the vessel wall to the interstitial space:

$$P_{ec} = \frac{\phi_V(1-\sigma_f)}{L_P \frac{S}{V}} \quad (24)$$

Since experimental evidences have revealed that there is no functional lymphatic system in tumor tissue, the sink item ϕ_L in Eq. (22) can be considered as:

$$\phi_L = \begin{cases} \phi_L C_d & \text{in normal tissue} \\ 0 & \text{in tumor tissue} \end{cases} \quad (25)$$

Finally, the general form of drug transport in the model is as follows:

$$\frac{\partial C_d}{\partial t} = \underbrace{\nabla \cdot (D_d \nabla C_d)}_{\text{diffusion in interstitium}} - \underbrace{\nabla (U_i C_d)}_{\text{convection in interstitium}} + \left(\underbrace{L_P \frac{S}{V} (C_d^P - C_d)}_{\text{diffusion rate across the vessel}} \left[\frac{P_{ec}}{e^{P_{ec}} - 1} \right] + \underbrace{\phi_V (1 - \sigma_f) C_d^P}_{\text{convection rate across the vessel}} \right) - \underbrace{\phi_L}_{\text{lymphatic item}} \quad (26)$$

To discrete the above equation with finite differential method, we can obtain the dynamic distribution of drug concentration in the simulation region.

2.4 Tumor growth model

The probabilistic cell automaton (CA) model is applied for tumor cell growth based on the previous work [Cai, Wu and Li et al. (2016)]. We assume four different phenotypes of glioma cells: the proliferating cells (PC), the quiescent cells (QC), and the necrotic cells (NC). Initially, we put 20 proliferating cells in the central area of the simulation domain. Two thresholds of oxygen concentration for cell proliferation (θ_{prol}) and cell survival (θ_{surv}) are introduced to describe the effects of oxygen field on the tumour cell actions. The relationships of the three phenotypes of tumor cells with the local microenvironment are shown in Figure 3. Each phenotype of tumor cell has a different coefficient of oxygen consumption rate and the production rate of VEGF and MDEs (Table 2) [Cai, Wu and Li et al. (2016)].

Table 2: Parameters of different phenotypes of tumor cells.

Phenotypes	MDE production	VEGF production	Oxygen consumption
proliferating cells (PC)	μ_T	χ	γ
quiescent cells (QC)	$\mu_T / 5$	$\chi \times 2$	$\gamma / 2$
necrotic cells (NC)	$\mu_T / 10$	$\chi \times 4$	$\gamma / 4$

To be specific, if the local oxygen ($C_o^{\text{ex}} \geq \theta_{\text{prol}}$) and a neighbouring space is available, a tumor cell will proliferate into two daughter cells with a probability, defined as $T_{\text{age}}/T_{\text{TC}}$.

T_{TC} is the tumor cell proliferation time (set to be 9 hours, equals to 6 time steps). T_{age} is the tumor cell age, ranging from 1 to T_{TC} and with an incremental 1 in each simulation time step. One of the two daughter cells will replace the parent cell and the other cell will move to a neighboring node space. When the local oxygen concentration at a tumor site is less than the cell survival threshold θ_{surv} , the tumour cell is marked as a necrotic cell and will not be revisited at the next time step. A necrotic cell has a probability of 20% to disappear and release the space for a tumor cell or an endothelial cell if it stays necrotic for more than 45 hours (30 times steps). When a tumor cell satisfies the survival condition but there is no neighboring space for it to proliferate, it will go quiescent. In the current model, there is no time limit for a cell to stay in the quiescent state. When the neighboring space of one quiescent cell has been released, the quiescent cell will turn back into a proliferating cell if the local oxygen supply is sufficient.

At every simulation step, the concentration of the chemotherapeutic drugs at every cell position is determined after the calculation of drug delivery modeling (section 2.3). The drug is assumed to be acted only with the proliferating cells and the quiescent cells. If the drug concentration at the cell node exceeds a specific threshold k_{drug} , the tumor cell will be killed. This is represented by removing the grid to an empty space, which may take neighboring quiescent cells with 'no space' marker back into an active proliferating phase.

2.5 Simulation algorithm

The schematic of main framework of the current model is shown in Fig. 2. At first, we initialize the model parameters listed in Table 3. A three-dimensional pre-existing vessel network is created as shown in Fig. 1A. Then we put 20 proliferating tumor cells with random ages in the central region. All chemicals' concentrations have been normalized to be between zero to one. The initial condition of ECM density is set to be 1 and other chemicals' concentrations (oxygen, VEGF and MDEs) are 0. No-flux boundary conditions are used in the simulation field. The drug concentration inside the microvessels can be predicted using pharmacokinetics models in the body level. For simplicity, we assumed the initial intravascular drug concentration as constant value of 2.13 mol/m^3 , which is commonly used for doxorubicin [Goh, Kong and Wang (2001)].

The tumor cell distribution and microvessel network are coupled by the dynamic changes of the chemical microenvironment and hemodynamical microenvironment. Since chemicals are transported much faster than the characteristic time for cell proliferation and migration, the chemicals' concentrations are solved to steady state at each time step of the simulation with an inner iteration step of 5s. It is noteworthy that the drug delivery model is carried out based on hemodynamic information such as interstitial fluid velocity.

The outputs of the present model include the distribution of tumor cells, microvasculature, concentrations of chemicals and drugs at any time point. In addition, the hemodynamic information can be examined. However, the main purpose of this study is to investigate the influence of vessel abnormality on the drug transport. The results of hemodynamics and chemicals are not shown in the following section. Readers may refer to our previous published paper [Cai, Xu and Wu et al. (2011); Cai, Wu and Li et al. (2016)] in which the

dynamic changes of chemical and hemodynamic microenvironment have been analyzed.

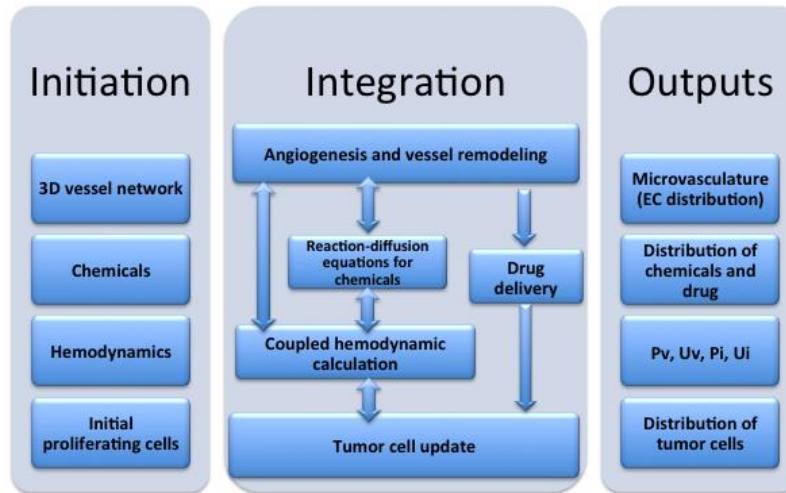


Figure 2: Main structure of the present model. A 3D microvessel network is generated with initial proliferating cells. The chemicals' concentration and the hemodynamic parameters are also initialized. The body of simulation involves the integration of several parts, as illustrated in Section 2.1-2.4. The outputs of the simulation results include the dynamic distribution of tumor cells, microvasculature, chemicals, and hemodynamic information.

Table 3: Parameter values used in the simulation.

Parameter	Value	Description	Reference
Δl	10 μ m	Lattice constant	
σ_T	0.82	Average osmotic reflection coefficient for plasma proteins	Baxter & Jain (1989)
π_V	20mmHg	Colloid osmotic pressure of plasma	Baxter & Jain (1989)
π_i	15mmHg	Colloid osmotic pressure of interstitial fluid	Baxter & Jain (1989)
K	4.13 $\times 10^{-8}$ cm ² /mmHg s	Hydraulic conductivity coefficient of the interstitium	Baxter & Jain (1989)
S/V	200cm ⁻¹	Surface area per unit volume for transport in the interstitium	Baxter & Jain (1989)
D_m	10 ⁻⁹ cm ² s ⁻¹	MDE diffusion coefficient	Anderson. (2005)

δ	$1.3 \times 10^2 \text{ cm}^3 \text{ M}^{-1} \text{ s}^{-1}$	ECM degradation coefficient	Cai et al. (2011)
μ_T	$1.7 \times 10^{-18} \text{ M cells}^{-1} \text{ s}^{-1}$	MDE production by TC	Cai et al. (2011)
μ_E	$0.3 \times 10^{-18} \text{ M cells}^{-1} \text{ s}^{-1}$	MDE production by EC	Cai et al. (2011)
λ	$1.7 \times 10^{-8} \text{ s}^{-1}$	MDE decay coefficient	Anderson. (2005)
α	$1.27 \times 10^{-15} \text{ } \mu\text{mol} / (\text{ } \mu\text{m}^3 \text{ mmHg})$	Bunsen solubility coefficient	Fang et al. (2008)
D_o	$10^{-5} \text{ cm}^2 \text{ s}^{-1}$	Oxygen diffusion coefficient	Anderson. (2005)
γ	$6.25 \times 10^{-17} \text{ M cells}^{-1} \text{ s}^{-1}$	Oxygen consumption coefficient	Anderson. (2005)
L_p^T	$2.8 \times 10^{-7} \text{ cm/mmHg s}$	Vessel permeability in tumour tissue	Baxter & Jain (1989)
E	6.5mmHg	Vessel compliance coefficient	Netti et al. (1996)
b	0.1	Vessel compliance index	Netti et al. (1996)
D_d	$1.5 \times 10^{-10} \text{ cm}^2 \text{ s}^{-1}$	Drug diffusion coefficient	Tang et al. (2014)
σ_f	0.9	Solvent-drag reflection coefficient	Sefidgar et al. (2015)

3 Results

3.1 Global growth history of tumor cells and microvasculature

Fig.3 shows the three-dimensional global views of the solid tumor and the microvasculature at different growing stage. The red tubes represent the microvessels, while the pink volume shows the invasion region of the tumor to the surrounding healthy tissue. At the early stage (T=20), few neo-vasculature can be found around the tumor. Most tumor cells proliferate around well-perfused areas, i.e., the pre-existing vessels, to obtain enough oxygen to their development. After angiogenesis phase is triggered on, the neo-capillaries arise at the tumor periphery (T=50) and form circulated vessels to support the rapid growth of the tumor. It is noteworthy that the tumor morphology has changed from nearly round to be more heterogeneous at T=100, which indicates that the irregular distribution

of angiogenic microvessels contributes to the invasive morphology of the tumor. At $T=150$, the tumor margin is almost fully covered by the neo-vasculature, which is consistent with the hypovascular region observed in both in vivo and in vitro experiments [Holash, Maisonpierre and Compton et al. (1999)].

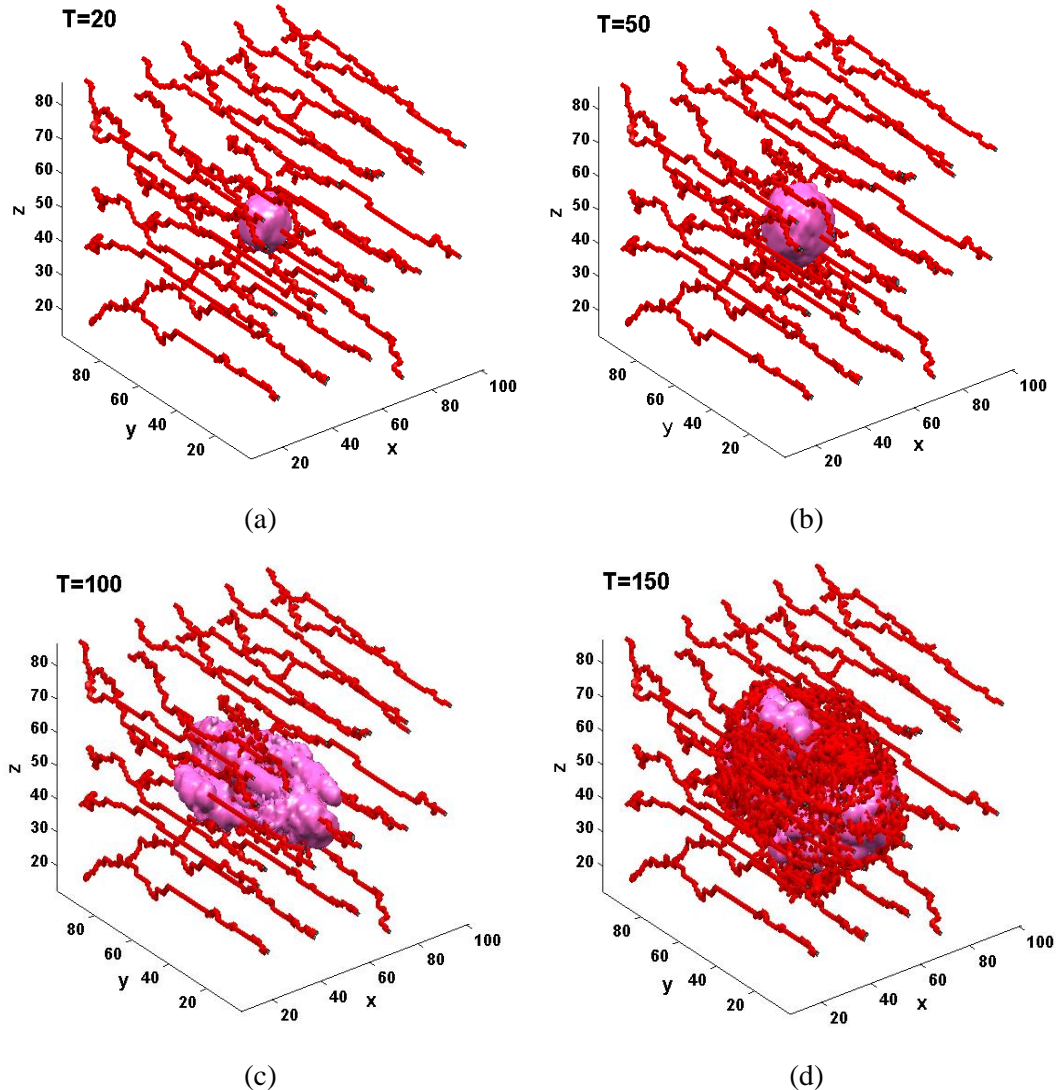


Figure 3: The three-dimensional global views of the solid tumor and the microvasculature at different growing stage. (a) $T=20$; (b) $T=50$; (c) $T=100$; (d) $T=150$. The red tubes represent the microvessels, while the pink volume shows the invasion region of the tumor to the surrounding healthy tissue.

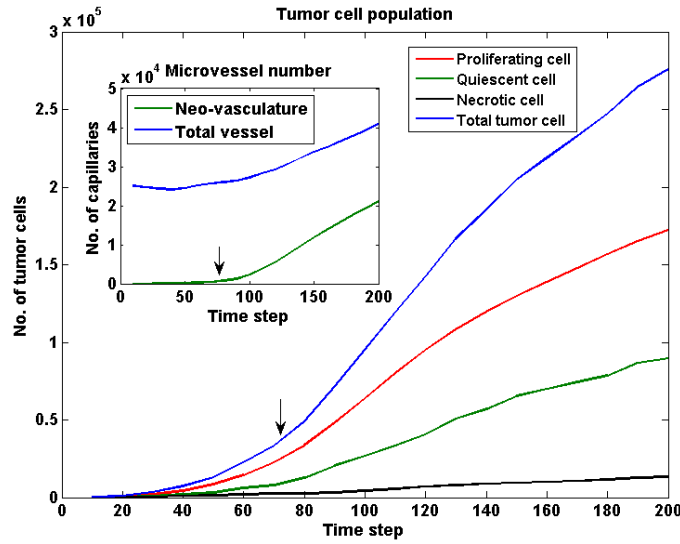


Figure 4: Growth curves of tumor cells with different phenotypes and microvessels (the inserted figure). The arrows represent the starting point of angiogenesis defined when the neo-vessels account for 5% of total vessel segments. The simulation ended at T=200 when the tumor size reached finishing criteria.

Fig. 4 shows the curves of different cell population over time. We can characterize the tumor growth process by two distinct stages according to the EC number: avascular stage and vascularized stage. In the present model, the starting point of angiogenesis for a simulation is defined when the neo-vessels account for 5% of total vessel segments (shown by the arrow in the inserted figure). After angiogenesis phase occurs (about T=75), the tumor is then in an accelerating development stage, which is reflected in the TC number curve. The number of necrotic cells is normally small, while population of the proliferating cells and quiescent cells are growing gradually with the increased angiogenic vessels. The simulation ended at T=200 when the tumor size reached finishing criteria.

3.2 Drug delivery and its effects on the tumor growth

The chemotherapy was simulated to start at T=50 and T=150 separately, corresponding to avascular phase and vascularized phase respectively. Fig. 5(a)(b) show the distribution of normalized drug concentration at plane $z=50$ after treatment. The highest drug concentration always occurs in the pre-existing vessels especially nearby the inlets of the vessel network. Although there are few functional microvessels inside the tumor center, the cytotoxic drug cannot transport very well in the tumor region, resulting in the large areas of low drug concentration and the heterogeneity in the whole distribution. The high concentration regions are scattered around the well-perfused functional vessels. The injection of the same doses of drug at vascularized phase (T=150) generally elevated the drug concentration to some extent, which suggests that sufficient circulated microvessels are needed in the drug delivery.

Fig. 5(c) (d) show the integrated drug concentration along the x-axis at plane $z=50$. The dotted line represents the average value of drug concentration. All values have been normalized to be

zero to one. Due to the poor blood perfusion and interstitial hypertension inside the tumor, the average drug concentration is very low ($<20\%$) in all simulations. In addition, the drug concentration in most tumor region is lower than the average value no matter the injection is operated in avascular stage or in vascularized stage.

The growth curves of sum tumor cells and proliferating cells with different drug strategies are shown in Fig.6. After the chemotherapeutic drug is injected in the circulation, the proliferating cells are killed immediately resulting in the reduction of total number of tumor cells and the inhibition of tumor growth (the arrows in Fig.6). It is important to note that the drug injection at the vascularized stage may cause a remarkable cell apoptosis (the red line in Fig. 6). Although the proliferation of tumors could speed up after chemotherapy at $T=150$, the whole number of tumor cells decreased up to 50K at the simulation ending time. This suggests that the introduction of chemotherapeutic drug at the vascularized stage seems more effective in tumor growth suppression.

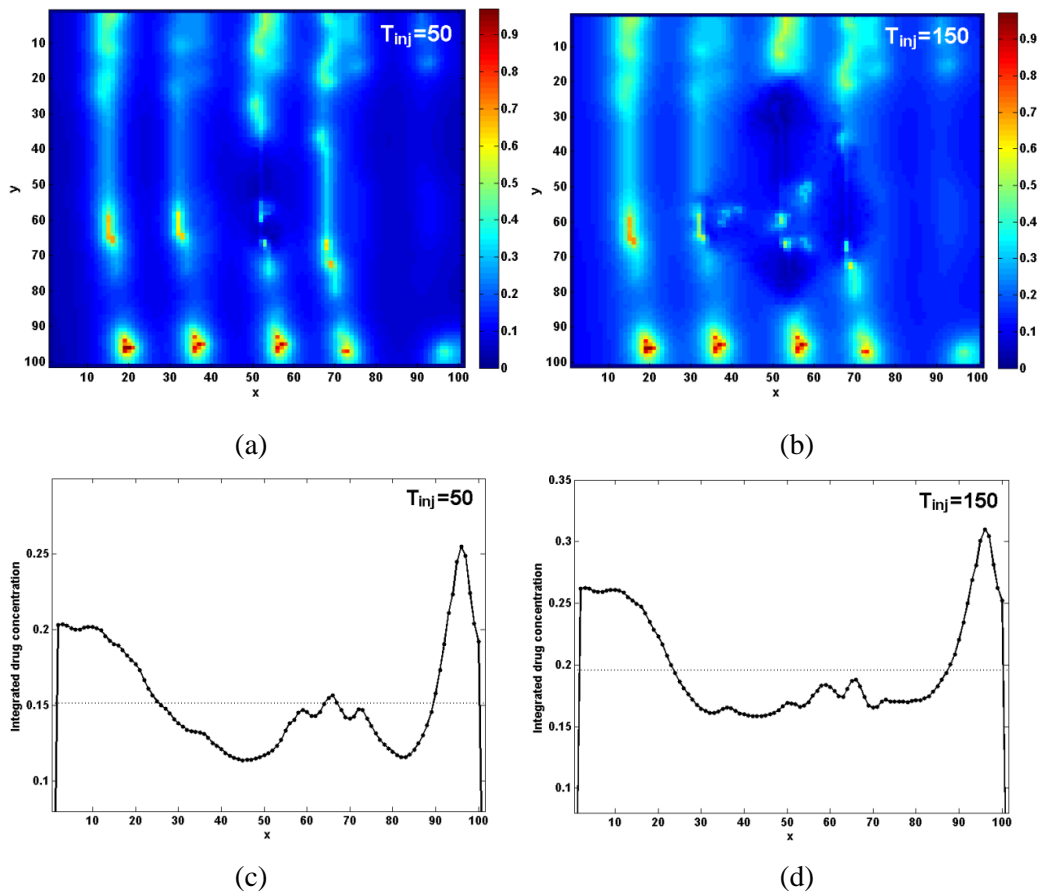


Figure 5: The chemotherapy was simulated to start at $T=50$ and $T=150$ separately, corresponding to avascular phase and vascularized phase respectively. (a) and (b) show the distribution of normalized drug concentration at plane $z=50$ after treatment. (c) and (d) show the integrated drug concentration along the x -axis at plane $z=50$. The dotted line represents the average value of drug concentration.

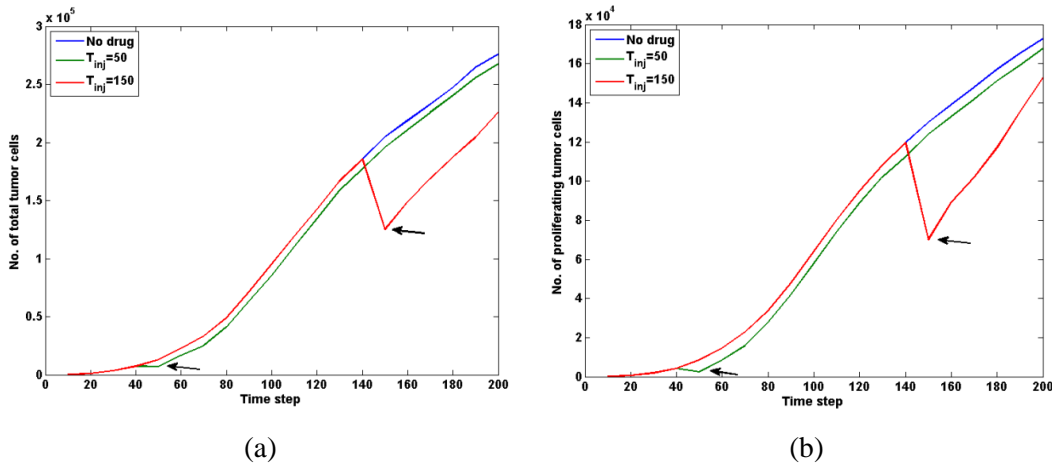


Figure 6: Growth curves of sum tumor cells and proliferating cells with different drug strategies. After the chemotherapeutic drug is injected in the circulation, the proliferating cells are killed immediately resulting in the reduction of total number of tumor cells and the inhibition of tumor growth (the arrows). It is important to note that the drug injection at the vascularized stage may cause a remarkable cell apoptosis (the red line).

3.3 Influence of abnormal vessel architecture on the drug delivery

3.3.1 Microvessel density

Additional simulations were performed with varied initial microvessel density (MVD) of pre-existing vessel network to study the influence of initial microvessel condition on the simulation results. The growth curves of proliferating tumor cells are presented in Fig. 7. The MVD of the baseline model is defined as MVD*, and the additional models are 1.5MVD* (More MVD case which has a MVD value 1.5 time larger than the baseline value) and 0.7MVD* (Less MVD case which has a MVD value of 0.7 time of the baseline value). The results of no drug model (Fig. 7(a)) show that the number of proliferating tumor cells in the three models have the same growing trend, while the values of them become smaller with decreasing MVD at the late stage of the simulations. When the chemotherapeutic drugs were injected at T=50, both the growth history and the final cell number have no significant changes with the no drug model (Fig. 7(b)). However, if the injection time is at the vascularized phase (T=150), the reduction of proliferating tumor cells is remarkable especially in the Less MVD case (the blue line in Fig. 7(c)). This result indicates that the decreasing of tumor microvessels by anti-angiogenic therapy may be helpful for improving the efficacy of combined chemotherapy.

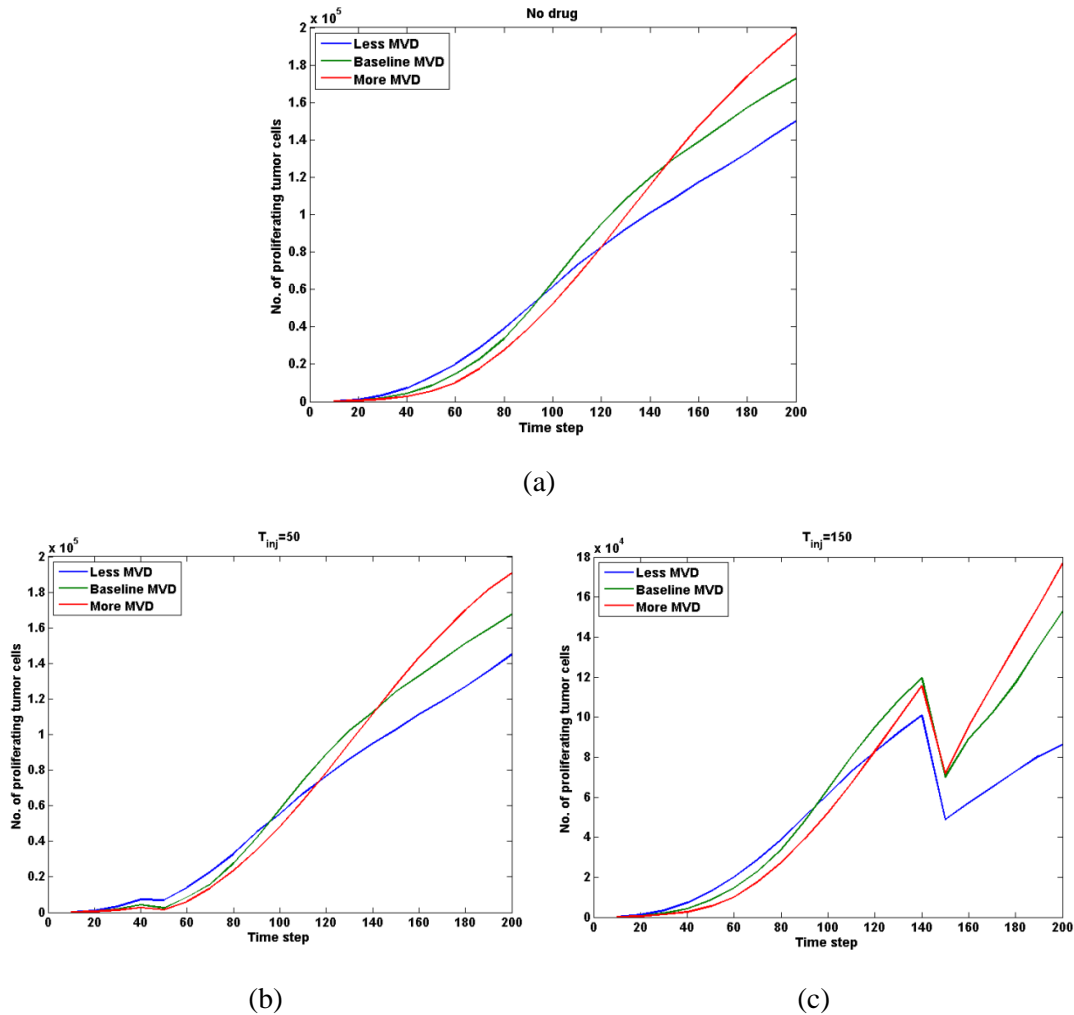


Figure 7: Growth curves of proliferating tumor cells in microvessel networks of different density. The MVD of the baseline model is defined as MVD^* , and the additional models are $1.5MVD^*$ (More MVD case which has a MVD value 1.5 time larger than the baseline value) and $0.7MVD^*$ (Less MVD case which has a MVD value of 0.7 time of the baseline value). (a) no drug injected; (b) drug injected at $T=50$; (c) drug injected at $T=150$.

3.3.2 The heterogeneity of the vessel diameter

The heterogeneity in tumor vessel diameter can increase the resistance to blood flow in tumors, which hinders the delivery and efficacy of therapeutic agents to tumors. In the presented model, the vessel remodeling including vessel dilation and vessel compression and collapse was introduced based on a series of complicated rules determined by the local microenvironment. To test the influence of vessel remodeling on the drug delivery, the settings of vessel remodeling are excluded in this section, i.e., the vessel diameter is

fixed based on the different Strahler order (Table 1). Fig. 8 shows the comparison of tumor growth history between Case A (baseline model, i.e., the vessel diameter is heterogeneous) and Case B (the vessel diameter is predefined by ordering without remodeling). It can be found that the average concentration of drug inside the tumor region has been elevated in Case B (see inserted figures), due to the decreasing resistance of blood perfusion in the well-organized microvasculature. The ordered vessel diameter has a great impact on the drug efficacy especially when the chemotherapy started at $T=150$. The reduction of tumor cell inhibition in an ordered vessel network is about 20K more than that in a heterogeneous vessel network.

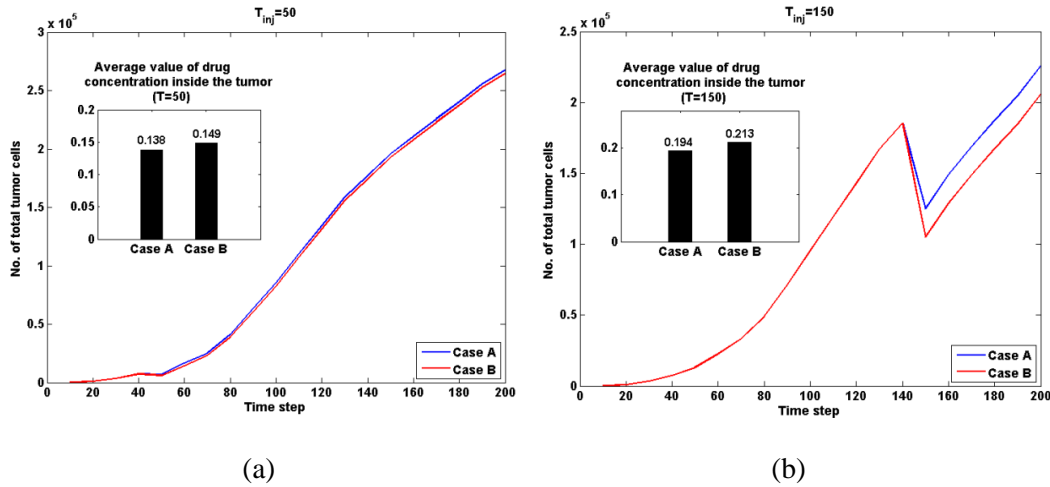


Figure 8: Growth curves of tumor cells in Case A (baseline model, i.e., the vessel diameter is heterogeneous) and Case B (the vessel diameter is predefined by ordering without remodeling). The inserted figures show the average value of drug concentration inside the tumor in Case A and Case B. (a) drug injected at $T=50$; (b) drug injected at $T=150$.

3.4 influence of interstitial hypertension on the drug delivery

The interstitial hypertension caused by the abnormal structure and function of blood and lymphatic vessels in tumors forms barriers to chemotherapy in two ways. On the one hand, reduced transmural pressure gradients decrease convection across the tumor vessel wall. On the other hand, the uniformly high interstitial fluid pressure compromises the drug delivery in the interstitium. Tumor vessels lack perivascular membrane and tight junctions resulting in the high vascular permeability, which is confirmed to be an important factor to elevate the interstitial fluid pressure. Therefore, we decreased the high permeability of tumor microvessels to study the influence of interstitial hypertension caused by the leaky abnormal vessels on the drug efficacy (Fig. 9). Specifically, the permeability of the vessel wall L_p in the baseline model is defined as L_p^* , while the ones in tested models are $0.1L_p^*$ and $0.01L_p^*$, respectively. It can be found that the average drug concentration inside the tumor increases with the reduced L_p , which demonstrates that the poor drug delivery has been improved by the normalization of the leaky tumor

microvessels. When the drug is injected at $T=150$, the influence of the reduced vessel permeability on the drug efficacy becomes more significant.

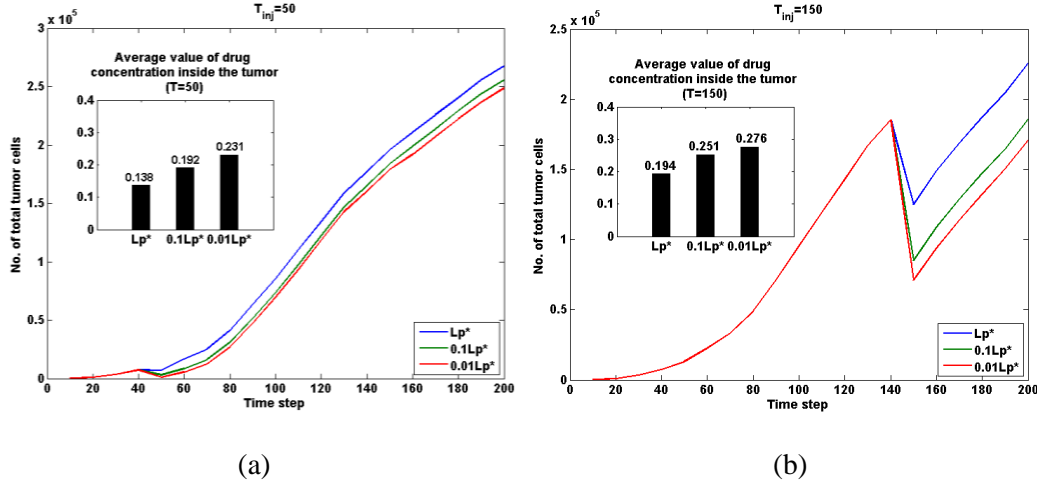


Figure 9: Growth curves of tumor cells with normalized permeability of tumor microvessels. Specifically, the permeability of the vessel wall L_p in the baseline model is defined as L_p^* , while the ones in tested models are $0.1L_p^*$ and $0.01L_p^*$, respectively. The inserted figures show the average value of drug concentration inside the tumor in different models. (a) drug injected at $T=50$; (b) drug injected at $T=150$.

4 Discussion and Conclusion

Tumor targeted delivery of a chemotherapeutic drug from the systemic circulation to the tumor is largely dependent on the tumor microcirculation. A growing tumor represents a dynamic microenvironment with changes in its cell mass, microvasculature, chemical substances, and other factors. They constitute together a barrier environment to tumor drug transport. To quantitatively study the role of tumor microvasculature in drug delivery in a dynamic growing tumor, we proposed a three-dimensional mathematical model system consisted of tumor growth, microvessel remodeling, blood perfusion and drug transport. The tumor growth is described by the cell automaton model, in which three cell phenotypes (proliferating cell, quiescent cell and necrotic cell) are assumed to reflect the dynamics of tumor progress. A 3D tree-like architecture network with different orders for vessel diameter is generated as pre-existing vasculature in host tissue. The chemical substances including oxygen, vascular endothelial growth factor, extra-cellular matrix and matrix degradation enzymes are calculated based on the reaction-diffusion equations associated with haemodynamic environment, which is obtained by coupled modeling of intravascular blood flow with interstitial fluid flow. The haemodynamic changes, including vessel diameter and permeability, are introduced to reflect a series of pathological characteristics of abnormal tumor vessels involving vessel dilation, leakage, angiogenesis, regression and collapse. The chemotherapeutic drug is transported across the vessel wall and through diffusion and convection mechanisms in the interstitial media, which is governed by the second Fick's law. Finally, we coupled the tumor growth model and

the vessel remodeling model according to the changes in the chemical and hemodynamical microenvironment, to investigate the tumor inhibition with different drug strategies.

The simulation results demonstrated the 3D tumor growth and invasion associated with vessel remodeling and angiogenesis. The chemotherapy was assumed to start at avascular phase and vascularized phase respectively. The growth curves of tumor cell population revealed that the injection of drugs at vascularized stage had more effective inhibition to tumor progress. Furthermore, the influences of abnormal characteristics of tumor microvessels on drug efficacy have been discussed, including microvessel density, heterogeneous vessel diameter and high permeability of vessel wall. The results showed that the normalization of above pathological factors can significantly improve the drug delivery inside the tumor by decreasing the resistances of blood perfusion in the tumor microcirculation.

The dynamic behavior of tumor microvessels plays an important role in anti-angiogenic therapy. Since the anti-angiogenic therapy is the idea that controlling the neoplastic growing by the reduction of nutrients supplies due to the inhibited angiogenic microvessels, one may infer that the decrease of the neo-vasculature by an anti-angiogenic agent might be detrimental for chemotherapy. However, more and more experimental and pre-clinical results confirmed the efficacy by combining chemotherapy with anti-angiogenic agent. To explain these findings, Jain hypothesized that the delivering of anti-angiogenic agent may regularize the abnormal vessel network with beneficial consequences for a successive chemotherapy [Fukumura and Jain (2007)]. Understanding of vessel “normalization” and its impact on anti-tumor drugs could require quantitative analysis of drug delivery in response to the dynamic microenvironment.

Systematic computational simulations by modifying different functional modules conducted in this paper illustrate the advantages of the current model. The model has the potential to incorporate additional details, including drug molecule properties and the cell response to drugs in subcellular level. We envision that the proposed model can serve as a predictive platform for designing the combination strategy of chemotherapy with anti-angiogenic therapy.

Acknowledgements: This research is supported by the National Basic Research Program of China (973 Program) (No. 2013CB733800), the National Nature Science Foundation of China (No. 11302050, No. 11272091), the Fundamental Research Funds for the Central Universities (YAN CAI, SEU), and ARC (FT140101152).

Conflict of interest: The authors declare that there is no conflict of interest regarding the publication of this paper.

References

- Anderson, A.R.A.; Chaplain, M.A.J.** (1998): Continuous and discrete mathematical models of tumor-induced angiogenesis. *Bull Math Biol*, vol. 60, pp.857-900.
- Anderson, A.R.A.** (2005): A hybrid mathematical model of solid tumour invasion: the

importance of cell adhesion. *Math Med Biol*, vol.22, pp.163-186.

Boucher, Y.; Baxter, L.T.; Jain, R.K. (1990): Interstitial pressure gradients in tissue-isolated and subcutaneous tumors: implications for therapy. *Cancer Research*, vol.50, pp. 4478-4484.

Baxter, L.T.; Jain, R.K. (1989): Transport of fluid and macromolecules in tumors. I. Role of interstitial pressure and convection. *Microvascular Res*, vol. 37, pp.77-104.

Cai, Y.; Xu, S., Wu, J.; Long, Q. (2011): Coupled modelling of tumour angiogenesis, tumour growth and blood perfusion. *J. Theor Biol.*, vol.276, pp. 90-101.

Cai, Y.; Wu, J.; Li, Z.; Long, Q. (2016): Mathematical modelling of a brain tumour initiation and early development: a coupled model of glioblastoma growth, pre-existing vessel co-option, angiogenesis and blood perfusion. *PLoS ONE*, vol.11, no.3, pp. e0150296.

Cassot, F.; Lauwers, F.; Fouard, C.; Prohaska, S.; Lauwers-Cances, V. (2006): A novel three-dimensional computer-assisted method for a quantitative study of microvascular networks of the human cerebral cortex. *Microcirculation*, vol.13, pp.1-18.

Deisboeck, T.S.; Berens, M.E.; Kansal, A.R.; Torquato, S.; Stemmer-Rachamimov, A.Q.; Chiocca, E.A. (2001): Pattern of self-organization in tumour systems: complex growth dynamics in a novel brain tumour spheroid model. *Cell Prolif*, vol.34, pp.115-134.

Danhier, F.; Feron, O.; Preat, V. (2010): To exploit the tumor microenvironment: passive and active tumor targeting of nanocarriers for anti-cancer drug delivery. *J. Controlled Release*, vol.148, pp.135-146.

Eberhard, A.; Kahlert, S.; Goede, V.; Hemmerlein, B.; Plate, K. H.; Augustin, H. G. (2000): Heterogeneity of angiogenesis and blood vessel maturation in human tumors: implications for antiangiogenic tumor therapies. *Cancer Research*, vol.60, pp.1388-1393.

Fukumura, D.; Jain, R.K. (2007): Tumor microvasculature and microenvironment: targets for anti-angiogenesis and normalization. *Microvasc Res*, vol.74, pp.72-84.

Fang, Q.; Sakadžić, S.; Ruvinskaya, L.; Devor, A.; Dale, A.M.; Boas, D. A. (2008): Oxygen advection and diffusion in a three dimensional vascular anatomical network. *Opt. Express*, vol.16, pp.17530-17541.

Goh, Y.; Kong, H.; Wang, C. (2001): Simulation of the delivery of doxorubicin to hepatoma. *Pharm. Res*, vol.18, pp.761-770.

Holash, J.; Maisonpierre, P. C.; Compton, D.; Boland, P.; Alexander, C. R.; Zaqzaq, D.; Yancopoulos, G. D.; Wiegand, S. J. (1999): Vessel cooption, regression, and growth in tumors mediated by angiopoietins and VEGF. *Science*, vol.284, pp.1994-1998.

Jain, R. K. (1990): Physiological barriers to delivery of monoclonal antibodies and other macromolecules in tumors. *Cancer Research*, vol.50, pp.814s-819s.

Knawar, I. A.; Kim, J. H.; Kuh, H. J. (2015): Improving drug delivery to solid tumors: priming the tumor microenvironment. *J. Control Release*, vol.201, pp.78-89.

Maeda, H.; Wu, J.; Sawa, T.; Matsumura, Y.; Hori, K. (2000): Tumor vascular permeability and the EPR effect in macromolecular therapeutics: a review. *J. Controlled Release*, vol. 65, pp. 271-284.

Mishra, S.; Katiyar, V. K.; Arora, V. (2007): Mathematical modeling of chemotherapy strategies in vascular tumor growth using nanoparticles. *Applied Math. Computation*, vol.

189, pp.1246-1254.

Moghadam, M. C.; Deyranlou, A.; Sharifi, A.; Niazmand, H. (2015): Numerical simulation of the tumor interstitial fluid transport: consideration of drug delivery mechanism. *Microvasc. Res*, vol.101, pp.62-71.

Narang, A. S.; Varia, S. (2011): Role of tumor vascular architecture in drug delivery. *Advanced Drug Delivery Reviews*, vol.63, pp. 640-658.

Netti, P.A.; Roberge, S.; Boucher, Y.; Baxter, L.T.; Jain, R.K. (1996): Effect of transvascular fluid exchange on pressure-flow relationship in tumors: a proposed mechanism for tumor blood flow heterogeneity. *Microvasc Res*, vol. 52, pp. 27-46.

Patlak, C.S.; Goldstein, D.A.; Hoffman, J.F. (1963): The flow of solute and solvent across a two-membrane system. *J. Theor. Biol*, vol. 5, pp. 426-442.

Penta, R.; Ambrosi, D. (2015): The role of the microvascular tortuosity in tumor transport phenomena. *J. Theor. Biol*, vol.364, pp. 80-97.

Rofstad, E. K.; Galappathi, K.; Mathiesen, B. S. (2014): Tumor interstitial fluid pressure-a link between tumor hypoxia, microvascular density, and lymph node metastasis. *Neoplasia*, vol.16, no.7, pp. 586-594.

Seo, B.R.; DelNero, P.; Fischbach, C. (2014): In vitro models of tumor vessels and matrix: engineering approaches to investigate transport limitations and drug delivery in cancer. *Advanced Drug Delivery Reviews*, vol. 69-70, pp.205-216.

Sefidgar, M.; Soltani, M.; Raahemifar, K.; Bazmara, H.; Nayinian, S. M.; Bazarqan, M. (2014): Effect of tumor shape, size, and tissue transport properties on drug delivery to solid tumors. *J. Biol. Eng*, vol.8, pp.12.

Sefidgar, M.; Soltani, M.; Raahemifar, K.; Sadeqhi, M.; Bazmara, H.; Bazarqan, M.; Mousavi Naeenian, M. (2015): Numerical modeling of drug delivery in a dynamic solid tumor microvasculature. *Microvasc. Res*, vol. 99, pp.43-56.

Tang, L.; van de Ven, A.L.; Guo, D.; Andasari, V.; Cristini, V.; Li, K.C.; Zhou, X. (2014): Computational modeling of 3D tumor growth and angiogenesis for chemotherapy evaluation. *PLoS ONE*, vol.9, no.1, pp. e83962.

Viallard, C.; Larrivé, B. (2017): Tumor angiogenesis and vascular normalization: alternative therapeutic targets. *Angiogenesis*, Jun 28, Doi: 10.1007/s10456-017-9562-9.

Welter, M.; Rieger, H. (2013): Interstitial fluid flow and drug delivery in vascularized tumors: a computational model. *PLoS ONE*, vol. 8, pp. e70395.

Wu, J.; Long, Q.; Xu, S.X.; Padhani, A.R. (2009): Study of tumor blood perfusion and its variation due to vascular normalization by anti-angiogenic therapy based on 3D angiogenic microvasculature. *J. Biomech*, vol.42, pp.712-721.

Welter, M.; Bartha, K.; Rieger, H. (2009): Vascular remodelling of an arterio-venous blood vessel network during solid tumour growth. *J. Theor. Biol*, vol. 259, pp.405-422.

Xu, X.; Farach-Carson, M.C.; Jia, X. (2014): Three-dimensional in vitro tumor models for cancer research and drug evaluation. *Biotechnology Advances*, vol. 32, pp.1256-1268.